Slow photoelectron velocity-map imaging of the C_nH^- (n = 5–9) anions

Etienne Garand,[a] Tara I. Yacovitch,[a] Jia Zhou,[a] Sean M. Sheehan[a] and Daniel M. Neumark*[ab]

Received 3rd February 2010, Accepted 22nd February 2010
DOI: 10.1039/c0sc00164c

High-resolution photoelectron spectra of the C_nH^- anions with n = 5–9 are acquired with slow electron velocity-map imaging (SEVI). Spectral features are assigned with the help of electronic structure calculations and Franck–Condon simulations. Well-resolved transitions to the linear $\tilde{X}^2\Pi$ and $\tilde{a}^4\Sigma^-$ neutral states are observed for species with an odd number of carbon atoms. For C_6H^- and C_8H^-, transitions to the $\tilde{X}^2\Pi$ neutral ground state and the low lying $\tilde{A}^2\Sigma^+$ excited state are observed. Precise electron affinities, term energies, fine structure splittings, and gas-phase vibrational frequencies are determined. The C_5H^-, C_7H^- and C_9H^- SEVI spectra are consistent with the anions having $\tilde{X}^3\Sigma^-$ linear triplet ground states.

Introduction

The linear carbon monohydride radical chains, C_nH, are important species in hydrocarbon combustion[1] and in the interstellar medium.[2] In both environments, these radicals serve as precursors for the formation of larger hydrocarbon chains and polycyclic species. The neutral chains with n = 2–8 have been observed in the circumstellar envelope of evolved stars,[3] where they can be formed by reactions of C and C_2 with unsaturated, closed-shell hydrocarbons.[3–5] The negatively charged carbon monohydrides C_4H^-, C_6H^-, and C_8H^- were among the first anions to be detected in interstellar and circumstellar media,[6–11] where they are formed by radiative attachment.[12] The chemistry of these species is closely coupled to their spectroscopy, motivating the work described in this paper, in which we continue our investigation of the carbon monohydride chains *via* negative ion photodetachment.[13–17] High resolution photoelectron spectra (PE) of the C_nH^- (n = 5–9) anions are measured using slow electron velocity-map imaging (SEVI). The SEVI spectra provide a detailed probe of the neutral and anionic states of these species, and yield insights into their geometries, vibronic structure, energetics, and the possibility of structural isomers.

Carbon monohydride radical chains have been the subject of numerous experimental and theoretical studies. Maier and co-workers have measured the UV-visible electronic absorption spectra of several neutral[2,18–23] and anionic[24–27] C_nH^- (n = 5–9) species in the gas phase and in rare-gas matrices. Thaddeus and co-workers have used Fourier transformed microwave (FTMW) spectroscopy and millimetre-wavelength absorption spectroscopy to study the neutral $C_{5-9}H$ species[28–36] as well as the C_6H^- and C_8H^- anions.[6,37] PE spectra of C_nH^- (n = 5, 6, 8) have also been reported.[13,16] Reaction kinetics and bond dissociation energies have been measured using flowing afterglow and guided ion beam mass spectrometry.[38,39] Many electronic structure calculations at various levels of sophistication have been carried out on the neutral and anionic carbon monohydrides in the size-range of interest here.[16,40–51]

This body of experimental and theoretical work has revealed significant differences in C_nH neutrals and anions depending on whether n is odd or even. In particular, there is evidence for multiple structural isomers for the odd-n anionic and neutral species. For example, theory and experiment indicate that the cyclic-C_3H isomer lies slightly lower in energy than the linear-C_3H isomer for both the anion and the neutral species.[17,52] Both linear and cyclic isomers of C_5H have been observed in microwave spectroscopy.[28,35] High level *ab initio* calculations[43,44] have identified the linear isomer of C_5H to be lower in energy. Using these energetics and PE spectroscopy, Sheehan *et al.*[16] recently suggested that a cyclic isomer was the lowest energy structure for the C_5H^- anion. Bowie and co-workers[46,53] have also reported the synthesis of several anionic and neutral isomers of C_5H and C_7H using mass spectrometry techniques and precursors with the proper bond connectivity.

In contrast, it is well-established that the neutral and anionic even-carbon C_nH species are linear. The anions have closed-shell $^1\Sigma^+$ ground states with strong acetylenic character.[48] The neutral species have low-lying $^2\Pi$ and $^2\Sigma^+$ states whose ordering switches with chain length.[13,40] The C_2H and C_4H radicals have $^2\Sigma^+$ ground-states, while the longer chains have $^2\Pi$ ground-states; the $\tilde{A}^2\Pi - \tilde{X}^2\Sigma^+$ splitting is only 213 cm^{-1} in C_4H.[15] The proximity of these two states in C_2H and C_4H leads to considerable spectral complexity attributed to strong vibronic coupling in both species,[14,15,54,55] while vibronic coupling in the longer chains with $\tilde{X}^2\Pi$ ground states has not been investigated.

In this paper, we report high resolution PE spectra of the C_nH^- anions, n = 5–9, acquired with SEVI.[56] These spectra are analyzed with the help of electronic structure calculations and Franck–Condon (FC) simulations. For all species, well-resolved vibrational and spin–orbit transitions to the linear $\tilde{X}^2\Pi$ ground state are observed. A second band of peaks is also observed for all species. It is assigned to the $\tilde{a}^4\Sigma^-$ excited state for C_5H, C_7H and C_9H and to the low-lying $\tilde{A}^2\Sigma^+$state for C_6H and C_8H. Several vibrational frequencies of the neutral species are determined for the first time. This work also demonstrates that the C_5H^-, C_7H^- and C_9H^- anions have $^3\Sigma^-$ linear ground states, in contrast to the bent structures previously reported.[16,46,53]

[a]*Department of Chemistry, University of California, Berkeley, California, USA. E-mail: dneumark@berkeley.edu; Fax: +1 (510) 642-3635; Tel: +1 (510) 642-3502*
[b]*Chemical Science Division, Lawrence Berkeley National Laboratory, Berkeley, California, 94720, USA*

Experimental

The SEVI apparatus has been described in detail elsewhere.[57,58] SEVI is a high resolution variant of PE spectroscopy in which mass-selected anions are photodetached at a series of wavelengths.[56] The resulting photoelectrons are collected by velocity-map imaging (VMI)[59,60] using relatively low extraction voltages, with the goal of selectively detecting slow electrons with high efficiency and enlarging their image on the detector. At each photodetachment wavelength, one obtains a high resolution photoelectron spectrum over a limited range of electron kinetic energies.

In this experiment, C_nH^- anions were produced from of a gas mixture comprising 1% acetylene and 1% propyne in a balance of Ar. The gas mixture, at a stagnation pressure of 300 psi, was expanded into the source vacuum chamber through an Even–Lavie pulsed valve[61] equipped with a grid discharge described in detail elsewhere.[62] Briefly, gas from the pulsed valve passed through a 2.5 mm × 23 mm channel made from Teflon and aluminium, within which were two fine grids made of stainless steel wire mesh and separated by 1 mm. The first grid was held to ground while the second was floated to around −500 VDC through a 1 kΩ resistor; the discharge was induced by passage of the expanding gas through the grids. Anions formed in the gas expansion were perpendicularly extracted into a Wiley–McLaren time-of-flight mass spectrometer and directed to the detachment region by a series of electrostatic lenses and pinholes. A pulse on the last ion deflector allowed only the desired mass into the interaction region.

Anions were photodetached between the repeller and the extraction plates of the VMI stack by the focused output of a Nd:YAG pumped tunable dye-laser. The photoelectron cloud formed was then coaxially extracted down a 50 cm flight tube and mapped onto a detector comprising a chevron-mounted pair of time-gated, imaging quality microchannel plates coupled to a phosphor screen, as is typically used in photofragment imaging experiments.[59] Events on the screen were collected by a 1024 × 1024 charge-coupled device (CCD) camera and sent to a computer. Electron velocity-mapped images resulting from 50 000–100 000 laser pulses were summed, quadrant symmetrized and inverse-Abel transformed.[63] Photoelectron spectra were obtained *via* angular integration of the transformed images. The spectra presented here are plotted with respect to electron binding energy (eBE), defined as the difference between the energy of the photodetachment photon and the measured electron kinetic energy (eKE).

The apparatus was calibrated by acquiring SEVI images of atomic Cl^- and S^- at several different photon energies, using the accurate electron affinities of these species reported previously.[64] With the −350 V VMI repeller voltage used in this study, the full widths at half maximum of the chloride peaks were 7.5 cm^{-1} at 150 cm^{-1} eKE and 18 cm^{-1} at 715 cm^{-1}. In the SEVI experiment, within the same image, all observed transitions have similar widths in pixels (Δr), so transitions observed further from threshold (larger r) are broader in energy. By varying the laser wavelength, a series of images in which the transitions of interest are close to the detachment threshold can be acquired, yielding a complete, high resolution photoelectron spectrum. Linewidths in the spectra presented here are limited by unresolved rotational structure. Since the origin of an unresolved rotational profile may not be aligned with the observed peak maximum, we report error bars of one Gaussian standard deviation for all energy determinations, typically 8 cm^{-1} for the highest resolution scans performed here.

SEVI also provides information on the photoelectron angular distribution (PAD). For one-photon detachment, the PAD is given by:[65,66]

$$\frac{d\sigma}{d\Omega} = \frac{\sigma_{total}}{4\pi}\left(1 + \beta P_2(\cos\theta)\right)$$

where θ is the angle between the direction of the photoelectron ejection and the polarization vector of the incident photon. The anisotropy parameter β lies between 2 and −1 and provides information on the orbital angular momentum (l) of the ejected photoelectron; $l = 0$ (s-wave) detachment leads to $\beta = 0$, $l = 1$ (p-wave) to $\beta = 2$, and $l = 0$ and 2 with equal amplitude and phase (s+d wave) to $\beta = -1$.

Results

SEVI spectra of the odd-carbon anions, C_5H^-, C_7H^- and C_9H^-, are shown in Fig. 1–3, while the SEVI spectra of the two even-carbon species, C_6H^- and C_8H^-, are shown in Fig. 4 and 5. The peak positions, shifts from the band origin, PADs, and assignments (see Analysis section) are summarized in Tables 1–5.

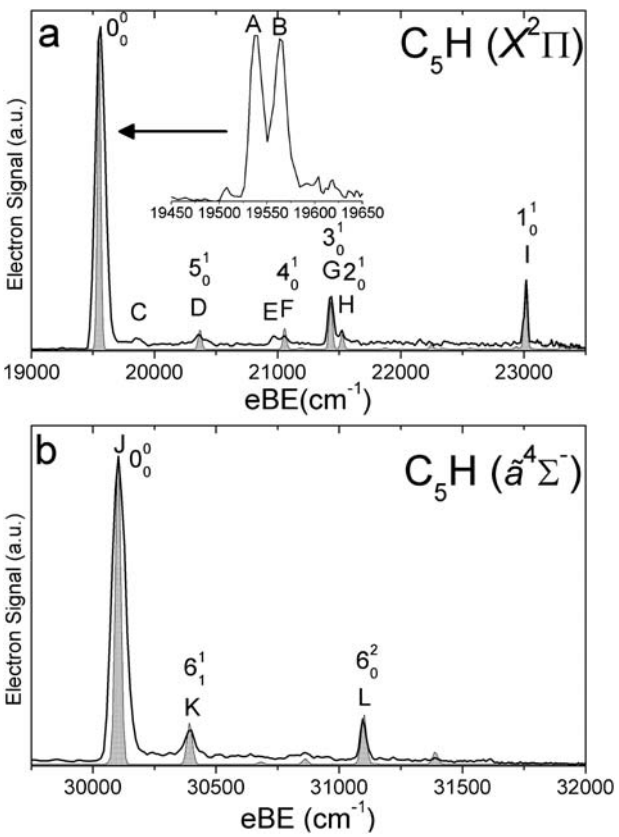

Fig. 1 SEVI spectra of C_5H^- covering the electron binding energy ranges of 19 000 to 23 500 cm^{-1} (panel a) and 29 500 to 32 000 cm^{-1} (panel b). Franck–Condon simulations show as gray-shaded peaks. Inset shows high-resolution scan of indicated feature.

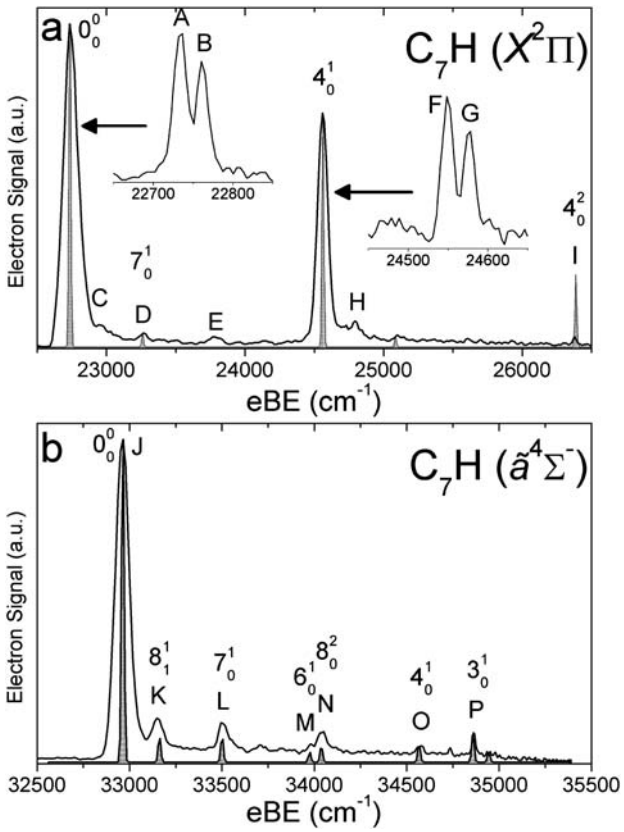

Fig. 2 SEVI spectra of C_7H^- covering the electron binding energy ranges of 22 500 to 26 500 cm^{-1} (panel a) and 32 500 to 35 500 cm^{-1} (panel b). Franck–Condon simulations show as gray-shaded peaks. Insets show high-resolution scans of indicated features.

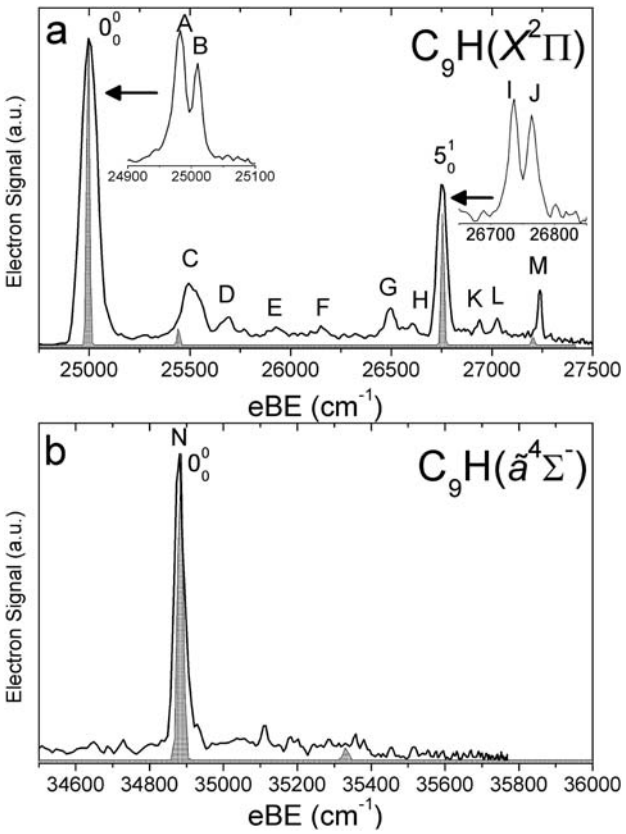

Fig. 3 SEVI spectra of C_9H^- covering the electron binding energy ranges of 24 750 to 27 500 cm^{-1} (panel a) and 34 500 to 35 800 cm^{-1} (panel b). Franck–Condon simulations show as gray-shaded peaks. Insets show high-resolution scans of indicated features.

Because the anisotropy parameter varies with photon energy,[67] we reported PADs as "*p*" or "*s*+*d*" for features having $\beta > 0$ and $\beta < 0$, respectively.

For each anion, panels a and b illustrate lower and higher eBE regions, respectively, of the SEVI spectra. Higher resolution SEVI traces taken at photon energies ~100–150 cm^{-1} above the feature at lowest eBE in the upper panels reveal each to be a closely spaced doublet, as shown in the insets in Fig. 1a–5a. These traces show doublet splittings of 25 cm^{-1}, 15 cm^{-1}, 27 cm^{-1}, 21 cm^{-1} and 30 cm^{-1} for C_5H^- to C_9H^-, respectively. Doublets with the same splittings were also resolved for the other intense transition in the first band of C_7H^- (peaks F and G) and C_9H^- (I and J). The same splittings are presumably found on other features in Fig. 1a–5a. However, their weak intensities prevented the acquisition of SEVI spectra sufficiently close to their respective detachment thresholds to observe these small splittings. No doublets were found in high resolution traces of the more intense features in Fig. 1b–5b.

In the C_5H^-, C_6H^-, C_7H^- and C_8H^- spectra, all the features in panel a have "*s*+*d*" PADs while those in panel b have "*p*" PADs. In the C_9H^- spectra, peaks A, B, I and J in Fig. 3a have "*s*+*d*" PADs, while the remaining smaller peaks all have "*p*" PADs. The single peak N in Fig. 3b also has a "*p*" PAD. In the SEVI spectra of C_5H^-, C_7H^- and C_9H^-, the lowest eBE transitions (peak A) of the first band are found at eBE of 19 539 cm^{-1}, 22 724 cm^{-1} and 24 980 cm^{-1}, respectively, while those of the second band are higher in energy by 10 502 cm^{-1}, 10 235 cm^{-1} and 9904 cm^{-1}, respectively. The large energy separation and different PADs indicate the features in panels a and b of Fig. 1–3 belong to different electronic states. Compared to the odd-carbon species, the SEVI spectra of C_6H^- and C_8H^- show higher electron binding energies for the lower energy band. The lower band origins are found at eBE of 30 722 cm^{-1} and 32 028 cm^{-1} in the C_6H^- and C_8H^- spectra, respectively, while the first bands in panel b are only 1492 cm^{-1} and 2112 cm^{-1} higher in energy. Although these relatively small energy intervals could represent vibrational frequencies, the different PADs for the features in panels a and b of Fig. 4–5 imply that the spectra in Fig. 4b and 5b are from transitions to low-lying excited electronic states of C_6H and C_8H, consistent with the assignment of earlier anion photoelectron spectra.[13]

For C_5H^-, C_6H^- and C_8H^-, the observed band structures and positions are consistent with the previously reported anion PE spectra.[13,16] However, the improved resolution of SEVI over conventional PE spectroscopy reveals numerous new features, especially in the lower bands of C_5H^- and C_6H^-. The SEVI spectra of C_7H^- and C_9H^- are the first photodetachment spectra reported for these species.

Computational details

Electronic structure calculations were performed on the relevant neutral and anionic states of C_nH. The current calculations serve

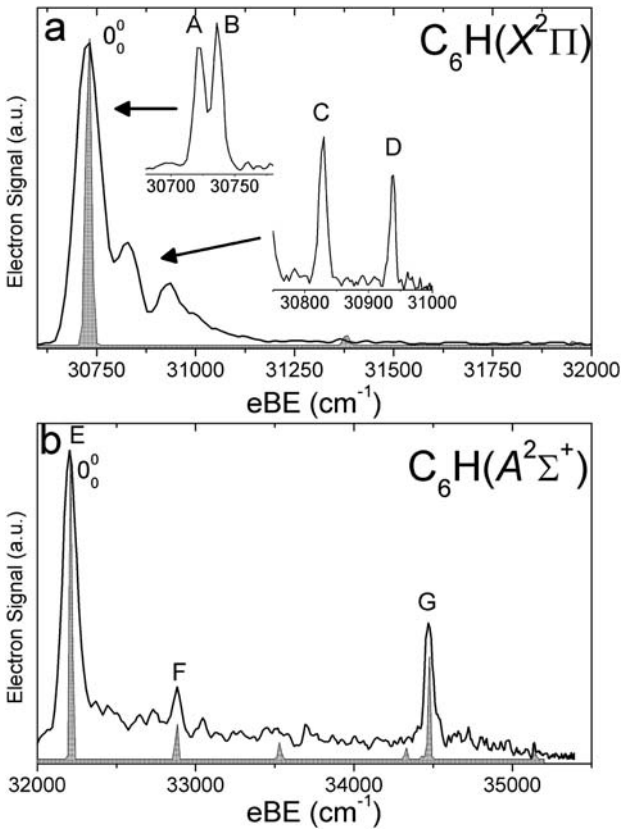

Fig. 4 SEVI spectra of C_6H^- covering the electron binding energy ranges of 30 600 to 32000 cm^{-1} (panel a) and 32 000 to 35 500 cm^{-1} (panel b). Franck–Condon simulations show as gray-shaded peaks. Inset shows high-resolution scan of indicated feature.

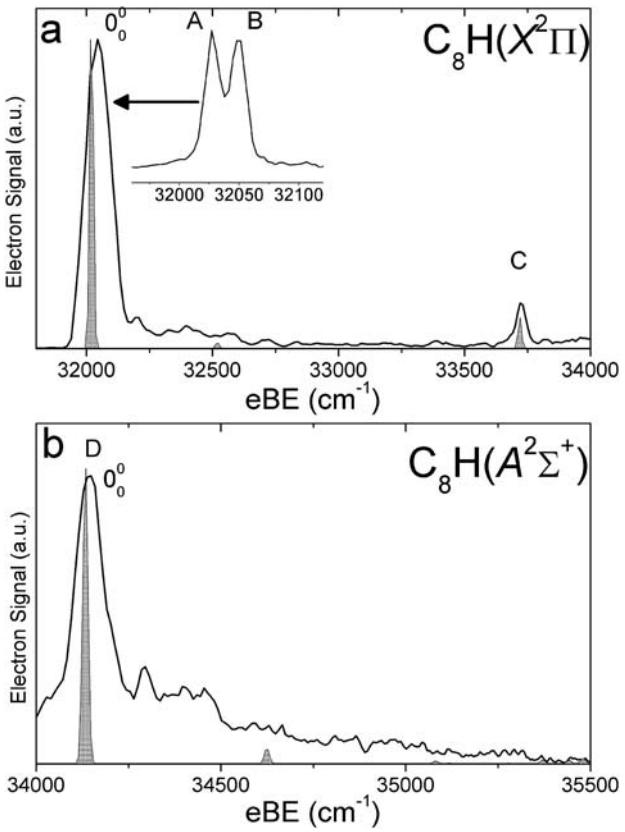

Fig. 5 SEVI spectra of C_8H^- covering the electron binding energy ranges of 31 750 to 34 000 cm^{-1} (panel a) and 34 000 to 35 500 cm^{-1} (panel b). Franck–Condon simulations show as gray-shaded peaks. Inset shows high-resolution scan of indicated feature.

to produce, at a uniform level of theory, all geometries, normal modes and vibrational frequencies necessary to perform Franck–Condon simulations and interpret the photoelectron spectra. Our calculations were carried out with density functional theory (DFT) using the Becke three-parameter Lee, Yang, and Parr exchange–correlation functional[68,69] (B3LYP) and the augmented correlation consistent polarized valence triple-zeta basis set[70] (AVTZ).

All computations were performed using the GAUSSIAN03 program.[71] Franck–Condon simulations were performed with the FCFgaus03 and PESCAL programs[72,73] using the Sharp–Rosenstock–Chen method[74] that treats all the modes as independent harmonic oscillators and relates the normal mode coordinates of the initial and final states *via* the Duschinsky transformation.[75] The calculated geometries and harmonic vibrational frequencies were used as a starting point for the FC simulations. The neutral frequencies were adjusted to the experimental values and the normal mode displacements were adjusted to fit the experimental spectra.

For C_5H^- and C_7H^-, several low-lying isomers with singlet and triplet spin multiplicity have been previously reported.[16,46,53] The carbon backbone of these isomers can be a single chain, a branched chain, or a branched three-membered ring. Consequently, we searched for the lowest energy isomers of C_5H^-, C_7H^- and C_9H^- by performing electronic structure calculations at the B3LYP/6-311+G level of theory on several different initial geometries for both the singlet and triplet surfaces. The lowest energy isomers were then re-optimized at the B3LYP/AVTZ level. We found that the isomer comprising a single carbon chain terminated by one hydrogen was lower in energy than the next-lowest isomer by 0.29 eV, 0.65 eV and 0.84 eV, for $n = 5$, 7, and 9, respectively. These lowest energy isomers were found to have a triplet ground state with the first singlet state lying higher in energy by 0.31 eV, 0.43 eV and 0.47 eV. The next-lowest isomers

Table 1 Peak positions, shifts from band origins, angular distributions (PAD), and assignments for the C_5H^- SEVI spectra

Peak	Position/ cm^{-1}	Shift/ cm^{-1}	PAD	Assignments (Vibs)	States
A	19 539	0	*s*+*d*	0^0_0	$\tilde{X}^2\Pi_{½} \leftarrow \tilde{X}^3\Sigma^-$
B	19 564	25	*s*+*d*	0^0_0	$\tilde{X}^2\Pi_{½} \leftarrow \tilde{X}^3\Sigma^-$
C	19 851	312	*s*+*d*	6^1_1	$\tilde{X}^2\Pi \leftarrow \tilde{X}^3\Sigma^-$
D	20 372	833	*s*+*d*	5^1_0	$\tilde{X}^2\Pi \leftarrow \tilde{X}^3\Sigma^-$
E	20 960	1421	*s*+*d*	6^2_0	$\tilde{X}^2\Pi \leftarrow \tilde{X}^3\Sigma^-$
F	21 060	1521	*s*+*d*	4^1_0	$\tilde{X}^2\Pi \leftarrow \tilde{X}^3\Sigma^-$
G	21 434	1895	*s*+*d*	3^1_0	$\tilde{X}^2\Pi \leftarrow \tilde{X}^3\Sigma^-$
H	21 527	1988	*s*+*d*	2^1_0	$\tilde{X}^2\Pi \leftarrow \tilde{X}^3\Sigma^-$
I	23 014	3475	*s*+*d*	1^1_0	$\tilde{X}^2\Pi \leftarrow \tilde{X}^3\Sigma^-$
J	30 101	0	*p*	0^0_0	$\tilde{a}^1\Sigma^- \leftarrow \tilde{X}^3\Sigma^-$
K	30 391	290	*p*	6^1_1	$\tilde{a}^1\Sigma^- \leftarrow \tilde{X}^3\Sigma^-$
L	31 098	997	*p*	6^2_0	$\tilde{a}^1\Sigma^- \leftarrow \tilde{X}^3\Sigma^-$

Table 2 Peak positions, shifts from band origins, angular distributions (PAD), and assignments for the C_7H^- SEVI spectra

Peak	Position/ cm^{-1}	Shift/ cm^{-1}	PAD	Assignments (Vibs)	States
A	22 734	0	*s*+*d*	0_0^0	$\tilde{X}^2\Pi_{½} \leftarrow \tilde{X}^3\Sigma^-$
B	22 761	27	*s*+*d*	0_0^0	$\tilde{X}^2\Pi_{½} \leftarrow \tilde{X}^3\Sigma^-$
C	22 957	223	*s*+*d*	8_1^1	$\tilde{X}^2\Pi \leftarrow \tilde{X}^3\Sigma^-$
D	23 258	524	*s*+*d*	7_0^1	$\tilde{X}^2\Pi \leftarrow \tilde{X}^3\Sigma^-$
E	23 776	1042	*s*+*d*	8_0^2	$\tilde{X}^2\Pi \leftarrow \tilde{X}^3\Sigma^-$
F	24 549	1815	*s*+*d*	4_0^1	$\tilde{X}^2\Pi_{½} \leftarrow \tilde{X}^3\Sigma^-$
G	24 576	1842	*s*+*d*	4_0^1	$\tilde{X}^2\Pi_{½} \leftarrow \tilde{X}^3\Sigma^-$
H	24 793	2059	*s*+*d*	$4_0^1 8_1^1$	$\tilde{X}^2\Pi \leftarrow \tilde{X}^3\Sigma^-$
I	26 379	3645	*s*+*d*	4_0^2	$\tilde{X}^2\Pi \leftarrow \tilde{X}^3\Sigma^-$
J	32 969	0	*p*	0_0^0	$\tilde{a}^4\Sigma^- \leftarrow \tilde{X}^3\Sigma^-$
K	33 149	180	*p*	8_1^1	$\tilde{a}^4\Sigma^- \leftarrow \tilde{X}^3\Sigma^-$
L	33 506	537	*p*	7_0^1	$\tilde{a}^4\Sigma^- \leftarrow \tilde{X}^3\Sigma^-$
M	33 980	1011	*p*	6_0^1	$\tilde{a}^4\Sigma^- \leftarrow \tilde{X}^3\Sigma^-$
N	34 041	1072	*p*	8_0^2	$\tilde{a}^4\Sigma^- \leftarrow \tilde{X}^3\Sigma^-$
O	34 572	1603	*p*	4_0^1	$\tilde{a}^4\Sigma^- \leftarrow \tilde{X}^3\Sigma^-$
P	34 863	1894	*p*	3_0^1	$\tilde{a}^4\Sigma^- \leftarrow \tilde{X}^3\Sigma^-$

Table 3 Peak positions, shifts from band origins, angular distributions (PAD), and assignments for the C_9H^- SEVI spectra

Peak	Position/cm^{-1}	Shift/cm^{-1}	PAD	Assignments (Vibs)	States
A	24 980	0	*s*+*d*	0_0^0	$\tilde{X}^2\Pi_{½} \leftarrow \tilde{X}^3\Sigma^-$
B	25 010	30	*s*+*d*	0_0^0	$\tilde{X}^2\Pi_{½} \leftarrow \tilde{X}^3\Sigma^-$
C	25 487	507	*p*		
D	25 671	691	*p*		
E	25 928	948	*p*		
F	26 157	1177	*p*		
G	26 495	1515	*p*		
H	26 603	1623	*p*		
I	26 735	1755	*s*+*d*	5_0^1	$\tilde{X}^2\Pi_{½} \leftarrow \tilde{X}^3\Sigma^-$
J	26 766	1786	*s*+*d*	5_0^1	$\tilde{X}^2\Pi_{½} \leftarrow \tilde{X}^3\Sigma^-$
K	26 934	1954	*p*		
L	27 024	2044	*p*		
M	27 236	2256	*p*		
N	34 884	9904	*p*	0_0^0	$\tilde{a}^4\Sigma^- \leftarrow \tilde{X}^3\Sigma^-$

Table 4 Peak positions, shifts from band origins, angular distributions (PAD), and assignments for the C_6H^- SEVI spectra

Peak	Position/ cm^{-1}	Shift/ cm^{-1}	PAD	Assignments (Vibs)	States
A	30 722	0	*s*+*d*	0_0^0	$\tilde{X}^2\Pi_{½} \leftarrow \tilde{X}^1\Sigma^+$
B	30 737	15	*s*+*d*	0_0^0	$\tilde{X}^2\Pi_{½} \leftarrow \tilde{X}^1\Sigma^+$
C	30 828	106	*s*+*d*		$\tilde{X}^2\Pi \leftarrow \tilde{X}^1\Sigma^+$
D	30 937	215	*s*+*d*		$\tilde{X}^2\Pi \leftarrow \tilde{X}^1\Sigma^+$
E	32 214	0	*p*	0_0^0	$\tilde{A}^2\Sigma^+ \leftarrow \tilde{X}^1\Sigma^+$
F	32 880	651	*p*	6_0^1	$\tilde{A}^2\Sigma^+ \leftarrow \tilde{X}^1\Sigma^+$
G	34 474	2260	*p*	2_0^1	$\tilde{A}^2\Sigma^+ \leftarrow \tilde{X}^1\Sigma^+$

also consisted of a single carbon chain, but with the hydrogen located on the third carbon for $n = 5$, 7 and the fifth carbon for $n = 9$. Hence, only triplet states with H-terminated carbon chains were analyzed in more detail for the odd-carbon anions, For the even-carbon species, only the well-known linear $^1\Sigma^+$ anion state and the accessible low-lying $^2\Pi$ and $^2\Sigma^+$ neutral states were considered.

Table 5 Peak positions, shifts from band origins, angular distributions (PAD), and assignments for the C_8H^- SEVI spectra

Peak	Position/ cm^{-1}	Shift/ cm^{-1}	PAD	Assignments (Vibs)	States
A	32 028	0	*s*+*d*	0_0^0	$\tilde{X}^2\Pi_{½} \leftarrow \tilde{X}^1\Sigma^+$
B	32 049	21	*s*+*d*	0_0^0	$\tilde{X}^2\Pi_{½} \leftarrow \tilde{X}^1\Sigma^+$
C	33 725	1697	*s*+*d*	5_0^1	$\tilde{X}^2\Pi \leftarrow \tilde{X}^1\Sigma^+$
D	34 140	2112	*p*	0_0^0	$\tilde{A}^2\Sigma^+ \leftarrow \tilde{X}^1\Sigma^+$

Calculated geometries and relative energies of the anionic and neutral states of the C_nH species are shown in Table 6, while harmonic vibrational frequencies are presented in Table 7. Vibrational mode labels for the neutral ground state are used throughout even if the ordering of the frequencies changes. For C_5H^-, the minimum energy structure is a $^3A'$ state with an almost linear carbon backbone and a CCH angle of 164.1°. However, the corresponding linear $^3\Sigma^-$ first-order transition state was found to be only 0.001 eV above the minimum energy structure. With such a small energy difference, the zero-point energy of the CCH bending mode certainly exceeds the barrier to linearity. Thus, the C_5H^- ground state will be considered to be the linear $^3\Sigma^-$ state with the expectation that this state is either quasilinear or has a very shallow CCH bending potential. This result differs from previous theoretical studies[16,46,76] using the same B3LYP functional with smaller basis sets that yielded strongly bent structures for the triplet ground-state of C_5H^-. This basis set effect might also explain why Blanksby *et al.*[46] did not find the chain isomer to be the lowest in energy by using single-point energy calculations at the RCCSD(T)/AVDZ level on the geometries obtained at the B3LYP/AVDZ level. For C_7H^- and C_9H^-, the truly linear $^3\Sigma^-$ state was found to be the minimum energy structure. This result is again in contrast with previous DFT studies[53,76] using smaller basis sets that found slightly bent structures for the triplet ground states of C_7H^- and C_9H^-.

All the neutral isomers considered here were found to have linear $^2\Pi$ ground-states. The calculated bond lengths in the ground states of C_5H, C_6H and C_7H are very similar to those obtained from microwave spectroscopy[36] and previous high level electronic structure calculations.[40,43] The calculations yield non-degenerate bending modes, as expected for vibrational modes of a $^2\Pi$ state subject to Renner–Teller (RT) coupling. For the neutral odd-carbon species, a linear $^4\Sigma^-$ excited state lying ~1.3 eV above the ground-state was found, similar to previous calculations on C_3H[17] and C_5H.[16] The calculated geometries for these $^4\Sigma^-$ states are similar to those of the $^3\Sigma^-$ anion state but with a shorter C_1–C_2 bond. For C_6H and C_8H, a low-lying $^2\Sigma^+$ excited state was found, in accordance with previous experimental and theoretical work.[13,40,47] The other observed or predicted excited states[18–21,23,44,47] of the linear neutral C_nH species are outside the energy range of the current study and thus were not considered theoretically here.

Analysis

In this section, detailed analyses and assignments of the SEVI spectral features are performed using the electronic structure

Table 6 Relative energies (eV, including zero-point correction) and geometries (Å, degrees) of the $C_{5-9}H$ anionic and neutral states calculated at the B3LYP/AVTZ level. The experimental (ref. 36) or recommended (ref. 48) bond lengths are shown in parentheses

Species	State	ΔE	Geometry								
C_5H			**C_1–C_2**	**C_2–C_3**	**C_3–C_4**	**C_4–C_5**	**C_5–H**	**$C_1C_2C_3$**	**$C_2C_3C_4$**	**$C_3C_4C_5$**	**C_4C_5H**
Anion	$\tilde{X}^3A'$	−2.56	1.284	1.302	1.305	1.25	1.061	180.0	179.5	176.9	164.1
	$^3\Sigma^{-a}$	−2.56	1.285	1.301	1.308	1.245	1.058				
Neutral	$\tilde{X}^2\Pi$	0.00	1.304	1.264	1.321	1.221	1.063				
			(1.308)	(1.267)	(1.329)	(1.224)	(1.055)				
	$\tilde{a}^4\Sigma^-$	1.35	1.253	1.287	1.311	1.23	1.061				
C_6H			**C_1–C_2**	**C_2–C_3**	**C_3–C_4**	**C_4–C_5**	**C_5–C_6**	**C_6–H**			
Anion	$\tilde{X}^1\Sigma^+$	−3.64	1.252	1.342	1.231	1.348	1.218	1.059			
			(1.2575)	(1.3518)	(1.2313)	(1.3581)	(1.2189)	(1.0594)			
Neutral	$\tilde{X}^2\Pi$	0.00	1.281	1.312	1.24	1.334	1.215	1.063			
			(1.257)	(1.332)	(1.237)	(1.341)	(1.216)	(1.056)			
	$\tilde{A}^2\Sigma^+$	0.60	1.21	1.355	1.214	1.354	1.207	1.061			
C_7H			**C_1–C_2**	**C_2–C_3**	**C_3–C_4**	**C_4–C_5**	**C_5–C_6**	**C_6–C_7**	**C_7–H**		
Anion	$\tilde{X}^3\Sigma^-$	−2.95	1.275	1.309	1.28	1.271	1.321	1.233	1.059		
Neutral	$\tilde{X}^2\Pi$	0.00	1.295	1.275	1.298	1.243	1.332	1.215	1.062		
			(1.301)	(1.273)	(1.309)	(1.243)	(1.341)	(1.217)	(1.057)		
	$\tilde{a}^4\Sigma^-$	1.31	1.241	1.304	1.281	1.259	1.326	1.221	1.061		
C_8H			**C_1–C_2**	**C_2–C_3**	**C_3–C_4**	**C_4–C_5**	**C_5–C_6**	**C_6–C_7**	**C_7–C_8**	**C_9–H**	
Anion	$\tilde{X}^1\Sigma^+$	−3.79	1.255	1.334	1.236	1.332	1.230	1.347	1.216	1.059	
			(1.2600)	(1.3440)	(1.2360)	(1.3435)	(1.2284)	(1.3592)	(1.2166)	(1.0598)	
Neutral	$\tilde{X}^2\Pi$	0.00	1.281	1.306	1.248	1.315	1.233	1.339	1.212	1.062	
	$\tilde{A}^2\Sigma^+$	0.71	1.212	1.351	1.218	1.343	1.218	1.352	1.208	1.062	
C_9H			**C_1–C_2**	**C_2–C_3**	**C_3–C_4**	**C_4–C_5**	**C_5–C_6**	**C_6–C_7**	**C_7–C_8**	**C_8–C_9**	**C_9–H**
Anion	$\tilde{X}^3\Sigma^-$	−3.25	1.271	1.312	1.268	1.284	1.294	1.256	1.330	1.225	1.059
Neutral	$\tilde{X}^2\Pi$	0.00	1.290	1.280	1.287	1.254	1.311	1.235	1.338	1.212	1.062
	$\tilde{a}^4\Sigma^-$	1.27	1.233	1.315	1.265	1.276	1.298	1.246	1.334	1.217	1.061

[a] Transition state.

Table 7 Calculated harmonic vibrational frequencies (cm^{-1}) at the B3LYP/AVTZ level of theory

State	ν_1	ν_2	ν_3	ν_4	ν_5	ν_6	ν_7	ν_8	ν_9	ν_{10}	ν_{11}	ν_{12}	ν_{13}	ν_{14}	ν_{15}	ν_{16}	ν_{17}
C_5H	**σ**	**σ**	**σ**	**σ**	**σ**	**π**	**π**	**π**	**π**								
$\tilde{X}^3\Sigma^-$	3473	1909	1790	1479	761	130i	456	396	135								
$\tilde{X}^2\Pi$	3449	2054	1952	1461	771	438/756	393/582	289/363	128/133								
$\tilde{a}^4\Sigma^-$	3453	1975	1721	1563	780	502	432	393	139								
C_6H	**σ**	**σ**	**σ**	**σ**	**σ**	**σ**	**π**	**π**	**π**	**π**	**π**						
$\tilde{X}^1\Sigma^+$	3480	2222	2142	1979	1206	641	483	550	494	264	111						
$\tilde{X}^2\Pi$	3451	2101	2132	1898	1224	650	574/701	512/554	393/466	191/245	89/107						
$\tilde{A}^2\Sigma^+$	3466	2285	2220	2114	1212	642	659	530	655	304	118						
C_7H	**σ**	**σ**	**σ**	**σ**	**σ**	**σ**	**σ**	**π**	**π**	**π**	**π**	**π**	**π**				
$\tilde{X}^3\Sigma^-$	3474	2023	1949	1769	1611	1071	564	334	488	470	387	198	81				
$\tilde{X}^2\Pi$	3453	2139	2051	1908	1581	1085	569	531/725	475/612	436/536	312/367	185/191	78/79				
$\tilde{a}^4\Sigma^-$	3455	2056	1999	1677	1628	1093	569	569	503	430	376	203	81				
C_8H	**σ**	**σ**	**σ**	**σ**	**σ**	**σ**	**σ**	**σ**	**π**	**π**	**π**	**π**	**π**	**π**	**π**		
$\tilde{X}^1\Sigma^+$	3478	2231	2200	2096	1982	1354	945	493	515	563	532	467	278	166	65		
$\tilde{X}^2\Pi$	3454	2189	2109	2044	1904	1373	959	499	604/694	543/595	508/528	399/447	248/266	145/162	62/63		
$\tilde{A}^2\Sigma^+$	3463	2279	2241	2174	2109	1346	947	491	654	619	572	493	318	178	66		
C_9H	**σ**	**σ**	**σ**	**σ**	**σ**	**σ**	**σ**	**σ**	**σ**	**π**	**π**	**π**	**π**	**π**	**π**	**π**	**π**
$\tilde{X}^3\Sigma^-$	3473	2072	2055	1945	1735	1658	1245	860	446	434	532	498	464	377	230	133	52
$\tilde{X}^2\Pi$	3454	2180	2130	2021	1850	1638	1255	869	448	583/706	563/663	485/580	438/506	322/364	218/224	126/131	49/50
$\tilde{a}^4\Sigma^-$	3457	2104	2048	2003	1735	1521	1260	869	448	600	588	498	420	348	235	134	51

Table 8 Experimentally determined electron affinities (eV), term energies (eV) and vibrational frequencies for the $C_{5-9}H$ species. Uncertainty is ±0.0010 eV for the energies and ±8 cm^{-1} for the vibrational frequencies

Species	State	Energy	ν_1	ν_2	ν_3	ν_4	ν_5	ν_6	ν_7	ν_8
C_5H	$\tilde{X}^3\Sigma^-$							208		
	$\tilde{X}^2\Pi$	EA = 2.4225	3462	1975	1882	1508	820			
	$\tilde{a}^4\Sigma^-$	T_0 = 1.3095						498		
C_6H	$\tilde{X}^2\Pi$	EA = 3.8090								
	$\tilde{A}^2\Sigma^+$	T_0 = 0.1751		2260				651		
C_7H	$\tilde{X}^3\Sigma^-$									356
	$\tilde{X}^2\Pi$	EA = 2.8187				1815			510	
	$\tilde{a}^4\Sigma^-$	T_0 = 1.2690			1894	1603		1011	537	536
C_8H	$\tilde{X}^2\Pi$	EA = 3.9701								
	$\tilde{A}^2\Sigma^+$	T_0 = 0.2619					1697			
C_9H	$\tilde{X}^2\Pi$	EA = 3.0971					1755			
	$\tilde{a}^4\Sigma^-$	T_0 = 1.2279								

calculations and FC simulations. Because of their different electronic character, leading to qualitatively different PE spectra, the odd- and even-carbon species will be considered separately. Peak assignments are shown in Tables 1–5, while experimentally determined electron affinities, term energies and vibrational frequencies are summarized in Table 8.

C_5H^-, C_7H^- and C_9H^-

In the C_5H^-, C_7H^- and C_9H^- SEVI spectra shown in Fig. 1–3, the splittings between the bands in the upper and lower panels are very similar to the calculated splittings in Table 6 between the neutral $\tilde{X}^2\Pi$ and $\tilde{a}^4\Sigma^-$ states. Both states are accessible from the $C_{2n+1}H^-$ ($n = 2$–4) $^3\Sigma^-$ ground states, which have a $[\ldots]\pi^4\pi^4\sigma^2\pi^2$ molecular orbital (MO) configuration. Removal of an electron from the highest occupied π or σ MO produces the neutral $\tilde{X}^2\Pi$ or $\tilde{a}^4\Sigma^-$state, respectively. As shown previously,[14,15,62] photodetachment from π and σ MOs often proceeds *via* "*s*+*d*" and "*p*" scattering, respectively. We thus assign the lower energy band of peaks to the $\tilde{X}^2\Pi$ neutral ground state and the second band to the $\tilde{a}\ ^4\Sigma^-$ first excited state, with both bands originating from the anion $\tilde{X}^3\Sigma^-$ state.

In the $\tilde{X}^2\Pi$ bands, the splitting of the vibrational origin into two closely spaced peaks, labeled A and B in Fig. 1a–3a, is attributed to spin–orbit coupling in the neutral vibrational ground state, and peaks A and B are assigned as transitions to the $\Pi_{1/2}$ and $\Pi_{3/2}$ spin–orbit components of this state. In C_5H and C_7H, the doublet splittings are 25 cm^{-1} and 27 cm^{-1}, respectively. These values are in good agreement with the spin–orbit splittings of 24.22 cm^{-1} and 26.17 cm^{-1} derived from FTMW and millimetre-wavelength absorption measurements[33,34] as well as the splittings seen in the visible $\tilde{A}^2\Delta \leftarrow \tilde{X}^2\Pi$ bands of C_5H and C_7H.[23] In C_9H, peaks A and B are spaced by 30 cm^{-1}; our spectrum is the first experimental determination of the spin–orbit splitting for this species. From the eBE of peak A, we obtain a refined electron affinity (EA) of C_5H and the first experimental EA of C_7H and C_9H. These values are EA(C_5H) = 2.4225 ± 0.0010 eV, EA(C_7H) = 2.8187 ± 0.0010 eV and EA(C_9H) = 3.0971 ± 0.0010 eV. The calculated EAs at the B3LYP/AVTZ level of theory, including zero-point energy corrections, are 2.56 eV, 2.95 eV and 3.25 eV for C_5H, C_7H and C_9H, respectively, as indicated in Table 6. Thus, the calculations systematically overestimate the EA of these species by around 0.15 eV.

FC simulations of the $\tilde{X}^2\Pi$ bands are shown as gray-shaded peaks in Fig. 1a–3a. Only the σ vibrational modes were included in these simulations; inclusion of the bending modes would require incorporating Renner–Teller coupling into the simulations and is beyond the scope of this work. The good agreement between the simulated and experimental spectra allows us to assign most of the observed features. In C_5H, peaks D, F, G and H are assigned to the 5_0^1, 4_0^1, 3_0^1 and 2_0^1 transitions, respectively. These four modes are all carbon backbone stretching vibrations. Peak I is assigned to the 1_0^1 transition in which the C–H stretching mode is excited. In C_7H, peak D is assigned to the 7_0^1 transition while peaks F and G are assigned to the $\Pi_{1/2}$ and $\Pi_{3/2}$ spin–orbit components of the 4_0^1 transition, respectively. Similarly, in C_9H, peaks I and J are assigned to the $\Pi_{1/2}$ and $\Pi_{3/2}$ spin–orbit components of the 5_0^1 transition, respectively. All of these modes are also carbon backbone stretching vibrations and their vibrational frequencies agree well with the calculated values.

Several smaller peaks are not reproduced by the FC simulations and are thus assigned to transitions involving bending modes. While the definitive assignments of these features would require a fuller understanding of RT coupling in these species, some tentative assignments can be made on the basis of the calculated harmonic bending vibration frequencies shown in Table 7. In C_5H and C_7H, the most likely active bending vibrations are the CCH bending modes (ν_6 and ν_8, respectively) because of the large changes in frequency between the anion and the neutral. This change in frequency would give rise to ν_0^2 transitions as well as ν_1^1 sequence bands located at higher eBE than the origin transition. For C_5H, peaks C and E could arise from the 6_1^1 and 6_0^2 transitions, while peaks C and E in the C_7H^- spectrum could be the 8_1^1 and 8_0^2 transitions. These assignments yield ν_6 frequencies (ignoring anharmonicities and RT effects) of 398 and 710 cm^{-1} in C_5H^- and C_5H, respectively, and ν_8 frequencies of 298 and 521 cm^{-1} for anionic and neutral C_7H. While these values are within range of our calculated frequencies in Table 7, evaluation of these assignments and frequencies is difficult because the calculated bend frequencies in the neutral are non-degenerate, the experimental levels have unknown RT splittings, and the calculation for C_5H^- yields an imaginary ν_6 frequency at the linear geometry.

The situation is different in the $\tilde{X}^2\Pi$ band of C_9H, where all the weaker transitions that are not reproduced by the FC simulations have a different PAD than the main spectral features (peaks A, B, I, and J). While these weaker features could originate from a different C_9H isomer, the lowest lying isomers of C_9H^- are calculated to lie more than 0.84 eV above the linear isomer and thus are unlikely to contribute to the spectrum. These

features are more likely to be nominally forbidden transitions to the $\tilde{X}^2\Pi$ state, such as bending vibrations with odd $\Delta\nu$, which gain intensity through vibronic coupling. In this case, those vibronically allowed transitions normally have the same PAD as the transitions to the electronic state from which intensity is borrowed.[14,77] The closest electronic state which can couple *via* bending modes with the $\tilde{X}^2\Pi$ state is the $\tilde{A}^2\Delta$ state. This state is expected to lie 1.88 eV above the ground state based on electronic structure calculations and extrapolations of the corresponding $\tilde{A}^2\Delta \leftarrow \tilde{X}^2\Pi$ transitions in C_5H and C_7H.[23] This term energy is 0.45 eV and 0.21 eV higher in C_5H and C_7H, respectively, providing a possible explanation as to why vibronic coupling effects appear stronger in C_9H than in the shorter chain species.

We next consider the $a^4\Sigma^-$ bands in Fig. 1b–3b. The dominant peak in each panel, labeled J in the C_5H^- and C_7H^- spectra and N in the C_9H^- spectrum, is assigned to the 0_0^0 transition. The term energies of the $a^4\Sigma^-$ states of C_5H, C_7H and C_9H are thus determined to be 1.3095 ± 0.0010 eV, 1.2690 ± 0.0010 eV and 1.2279 ± 0.0010 eV, respectively. These values are in excellent agreement with our calculations that predicted $a^4\Sigma^-$ term energies of 1.35 eV, 1.31 eV and 1.27 eV for these species. FC simulations, shown in shaded gray in Fig. 1b–3b, result in assignments of all the remaining features in the $a^4\Sigma^-$ bands of C_5H and C_7H.

In the C_5H^- spectrum, peaks K and L can be reproduced in the FC simulation by assigning them to the 6_1^1 and 6_0^2 transitions, respectively, by assigning a frequency of 208 cm^{-1} for the corresponding anion bending mode, and by setting the anion vibrational temperature to 150 K. This assignment of peak L yields a value of 498 cm^{-1} for the ν_6 fundamental of the $a^4\Sigma^-$ state, close to our calculated value of 502 cm^{-1} (Table 6). The low ν_6 anion frequency implied by this assignment is consistent with the very shallow CCH bending potential of C_5H^- inferred from our calculations. This anion frequency is preferable to that inferred from our assignment of peak C in the $\tilde{X}^2\Pi$ band, given the absence of RT splittings in the $a^4\Sigma^-$ band.

Similar CCH bending activity is found in the SEVI spectrum of C_7H^- where peaks K and N are assigned to the $8_1^1$and 8_0^2 transitions, respectively. These assignments of peak yield 356 cm^{-1} and 536 cm^{-1} for the anion and neutral ν_8 fundamentals (CCH bend), both of which are in reasonable agreement with calculated values in Table 7. The remaining peaks in the C_7H^- spectrum, labeled L, M, O and P, are assigned to the 7_0^1, 6_0^1, $4_0^1$and 3_0^1 transitions, respectively. These modes are all stretching vibrations of the carbon backbone and their frequencies are in good agreement with the calculated values.

C_6H^- and C_8H^-

In the $C_6H^-$and C_8H^- SEVI spectra shown in Fig. 4 and 5, the lower energy band is assigned to the $\tilde{X}^2\Pi$ neutral ground state and the second band to the $\tilde{A}^2\Sigma^+$ first excited state. Both states are accessible from the C_6H^- and C_8H^- $\tilde{X}^1\Sigma^+$ ground states, which have a $[\ldots]\pi^4\pi^4\sigma^2\pi^4$ MO configuration. Removal of an electron from the highest occupied π or σ MO produces the neutral $\tilde{X}^2\Pi$ or $\tilde{A}^2\Sigma^+$ state, respectively. As discussed earlier, photodetachment from π and σ MOs often proceeds *via* "*s*+*d*" and "*p*" scattering, respectively, consistent with the observed PADs.

In the $\tilde{X}^2\Pi$ bands, the two closely spaced peaks, labeled A and B in Fig. 4a–5a, are assigned as transitions to the $\Pi_{3/2}$ and $\Pi_{1/2}$ spin–orbit components, respectively, of the vibrational ground state. The splittings between those two peaks are 15 cm^{-1} and 21 cm^{-1}, in good agreement with the spin–orbit splittings of −15.11 cm^{-1} and −19.33 cm^{-1} derived from FTMW and millimetre wavelength absorption measurements[33,34] on C_6H and C_8H, respectively. From the eBE of the peaks labeled A, we obtain refined EAs for these two species: EA(C_6H) = 3.8090 ± 0.0010 eV and EA(C_8H) = 3.9701 ± 0.0010 eV. These values are within the uncertainties of those previously determined by Taylor *et al.*[13] They are also close to the calculated EAs, at the B3LYP/AVTZ level, of 3.64 eV and 3.79 eV for C_6H and C_8H, respectively.

The dominant peaks E and D in Fig. 4b and 5b, respectively, are assigned to the 0_0^0 transitions of the $\tilde{A}^2\Sigma^+$ state. The term energies of the first excited state are thus determined to be 0.1751 ± 0.0010 eV and 0.2619 ± 0.0010 eV, for C_6H and C_8H respectively. These values are within the uncertainties of the term energies reported by Taylor *et al.*[13] They are smaller than our calculated term energies of 0.60 eV and 0.71 eV for these species. However, the C_6H $\tilde{A}^2\Sigma^+$ state experimental term energy is in good agreement with the vertical transition energy of 0.22 eV calculated by Cao and Peyerimhoff.[47]

The C_6H^- and C_8H^- SEVI spectra display little vibrational activity. Some vibrational transitions can be assigned with the FC simulations, the results of which are shown in shaded gray in Fig. 4 and 5. In the $\tilde{A}^2\Sigma^+$ band of C_6H, peaks F and G are assigned to the 6_0^1 and 2_0^1 transitions, respectively. In the $\tilde{X}^2\Pi$ band of C_8H, peak C is assigned to the 5_0^1 transition.

Peaks C and D in the $\tilde{X}^2\Pi$ band of C_6H are not reproduced by the FC simulations and are thus assigned to bending vibrational modes. Again, the definitive assignment of these features would require a fuller understanding of the RT coupling in C_6H. Peaks C and D are shifted by only 106 cm^{-1} and 215 cm^{-1} from the origin. These positions roughly correspond to the calculated frequencies of the ν_{10} and ν_{11} modes. However, transitions to non-totally symmetric modes with odd $\Delta\nu$ are nominally forbidden, even in the presence of RT coupling. These peaks could be the 11_0^2 and 10_0^2 transitions; such an assignment would imply that the ν_{11} and ν_{12} frequencies are much smaller than the calculated values or that the RT coupling for these modes is very strong.

Another possibility is that peaks C and D are $\Delta\nu = 1$ bending transitions that gain intensity through vibronic coupling with the nearby $\tilde{A}^2\Sigma^+$ state, similar to what was observed in the SEVI spectra[14,15] of C_2H^- and C_4H^-. Usually, we would expect these features to have "*p*" PADs, similar to the features associated with the $\tilde{A}^2\Sigma^+$ state,[14] and not the observed "*s*+*d*" PADs. However, in the SEVI spectrum of C_4H^-, features were assigned to vibronically allowed $\Delta\nu = 1$ bending transitions even though the PADs were the same as for nearby, fully allowed transitions.[15]

Discussion

This study addresses the key issue of the structure of C_nH^- anions with an odd number of carbon atoms. Previous DFT studies on C_5H^-, $C_7H^-$and C_9H^- have reported bent geometries for the triplet ground state of the isomer comprising a single carbon chain terminated by a hydrogen.[16,46,53,76] In contrast, the

electronic structure calculations presented here predict a quasi-linear geometry for C_5H^- and linear geometries for $C_7H^-$and C_9H^-. The FC simulations involving transitions from these calculated linear $^3\Sigma^-$ anion ground electronic states to the $\tilde{X}^2\Pi$ and $\tilde{a}^4\Sigma^-$ neutral states were found to be in excellent agreement with the well-resolved features of the SEVI spectra. The $\tilde{X}^2\Pi$ states of C_5H, C_7H and C_9H, which can be unambiguously identified from the resolved spin–orbit splitting, are known to be linear from FTMW spectroscopy.[33,36] The observed small vibrational activity in the $\tilde{X}^2\Pi$ band is therefore consistent with linear-to-linear transitions. If the anion had a bent geometry, extensive bending progressions would be expected.[78] We thus conclude that the triplet ground states of the C_5H^-, $C_7H^-$and C_9H^- anions are linear, in accordance with our electronic structure calculations.

Another issue addressed here is the energy ordering of the various isomers of the odd-carbon anion species. For C_5H^-, a theoretical study by Blanksby *et al.*[46] found two isomers to be more stable than the single chain with terminal hydrogen (*l*-C_5H^-) discussed here. One isomer has a hydrogen located on the middle of a single carbon chain ($C_2[CH]C_2^-$, $^1A_1$), and the other a branched three-membered ring with the hydrogen located on the ring ([*c*-$C_3H]C_2^-$, $^1A'$); they were found to be 0.15 eV and 0.12 eV below *l*-C_5H^-, respectively. A third isomer, consisting of a branched three-membered ring with the hydrogen located at the end of the branch ([*c*-$C_3]C_2H^-$, $^1A_1$), was found to lie 0.13 eV above *l*-C_5H^-. A recent PE study of C_5H^- invoked the presence of both *l*-C_5H^- and [*c*-$C_3]C_2H^-$ isomers in order to assign all the observed spectral features. Based on their electron affinities and the calculated energetics of the neutral C_5H isomers,[43] the [*c*-$C_3]C_2H^-$ isomer was assigned to lie 0.16 eV below the *l*-C_5H^- isomer.

The electronic structure calculations and the C_5H^- SEVI spectra presented here point toward a somewhat different conclusion. First, the B3LYP/AVTZ calculations predict that *l*-C_5H^- is the most stable isomer by 0.29 eV. Secondly, only the *l*-C_5H^- isomer was necessary to assign the all the observed spectral features in the C_5H^- SEVI spectra. The main difference between the analysis of the current SEVI spectra and the previous PE spectra comes from the linear $^3\Sigma^-$ *l*-C_5H^- anion geometry used in the FC simulations instead of the bent $^3A'$ geometry. The large vibrational activity expected for a bent-to-linear transition was not compatible with some of the observed features in the PE spectrum and these were thus assigned to a cyclic isomer. Since the current study used short chain precursors (acetylene and propyne) that would not have hindered the formation of the various isomers, we conclude that the *l*-C_5H^- ($^3\Sigma^-$) isomer is the lowest energy structure on the C_5H^- potential energy surface. Similar conclusions can be reached for the *l*-C_7H^- ($^3\Sigma^-$) and *l*-C_9H^- ($^3\Sigma^-$) isomers on the same basis of the present DFT calculations and the analysis of the C_7H^- and C_9H^- SEVI spectra.

Our SEVI spectra also probe vibronic coupling in the carbon monohydrides. In C_2H, the small 3600 cm^{-1} spacing between the $\tilde{X}^2\Sigma^+$ and $\tilde{A}^2\Pi$ states results in strong pseudo-Jahn–Teller coupling that is well-documented and understood.[14] For C_4H, the $\tilde{X}^2\Sigma^+$ state lies only 213 cm^{-1} below the $\tilde{A}^2\Pi$ state which presumably yields even larger perturbations of the vibronic levels,[15] but these effects have not been theoretically addressed yet. For the larger even-carbon species studied here, the ordering of the two states is reversed and the splittings are 1492 cm^{-1} and 2112 cm^{-1} for C_6H and C_8H, respectively. While the appearance of peaks C and D in the C_6H^- SEVI spectra might be an indication of vibronic coupling, depending on their assignments, no indication of vibronic coupling is found in the C_8H spectra. This suggests that the amplitude of pseudo-Jahn–Teller coupling between the low-lying $^2\Sigma^+$ and $^2\Pi$ states of the even-carbon is small in C_6H and even smaller in the longer chains. The situation is reversed in the odd-carbon species; evidence of vibronic coupling is found in the SEVI spectra of C_9H^- but not in the spectra of the smaller chain species. If this coupling occurs between the $\tilde{X}^2\Pi$ and the $\tilde{A}^2\Delta$ states, as proposed above, vibronic coupling could be increasingly important for the longer-chain odd-carbon species because the $\tilde{X}^2\Pi$–$\tilde{A}^2\Delta$ splitting decreases with chain-length.[23]

Conclusions

High-resolution photoelectron spectra of the $C_{5-9}H^-$ species acquired with SEVI are reported. The spectra of C_5H^-, C_7H^-, and C_9H^- show well resolved transitions to the $\tilde{X}^2\Pi$ and $\tilde{a}^4\Sigma^-$ neutral states. For C_6H^- and C_8H^-, transitions to the $\tilde{X}^2\Pi$ and $\tilde{A}^2\Sigma^+$ neutral states are observed. Most of the observed spectral features are assigned with the help of electronic structure calculations and FC simulations. Precise electron affinities and term energies are determined and several gas-phase vibrational frequencies are determined for the first time. For the odd-carbon species, the observed spectral features and electronic structure calculations are consistent with linear $\tilde{X}^3\Sigma^-$ ground states for the anions, with no other isomers contributing to the spectra.

Acknowledgements

This work was supported by the Air Force Office of Scientific Research under Grant No. F49620-03-1-0085. E.G. and T.Y. both thank the National Science and Engineering Research Council of Canada (NSERC) for a postgraduate scholarship.

Notes and references

1 J. H. Kiefer, S. S. Sidhu, R. D. Kern, K. Xie, H. Chen and L. B. Harding, *Combust. Sci. Technol.*, 1992, **82**, 101–130.
2 E. B. Jochnowitz and J. P. Maier, *Mol. Phys.*, 2008, **106**, 2093–2106.
3 L. M. Ziurys, *Proc. Natl. Acad. Sci. U. S. A.*, 2006, **103**, 12274–12279.
4 X. B. Gu, Y. Guo, F. T. Zhang, A. M. Mebel and R. I. Kaiser, *Faraday Discuss.*, 2006, **133**, 245–275.
5 R. I. Kaiser, C. Ochsenfeld, D. Stranges, M. Head-Gordon and Y. T. Lee, *Faraday Discuss.*, 1998, **109**, 183–204.
6 M. C. McCarthy, C. A. Gottlieb, H. Gupta and P. Thaddeus, *Astrophys. J.*, 2006, **652**, L141–L144.
7 S. Brunken, H. Gupta, C. A. Gottlieb, M. C. McCarthy and P. Thaddeus, *Astrophys. J.*, 2007, **664**, L43–L46.
8 J. Cernicharo, M. Guelin, M. Agundez, K. Kawaguchi, M. McCarthy and P. Thaddeus, *Astron. Astrophys.*, 2007, **467**, L37–L40.
9 Y. Kasai, E. Kagi and K. Kawaguchi, *Astrophys. J.*, 2007, **661**, L61–L64.
10 A. J. Remijan, J. M. Hollis, F. J. Lovas, M. A. Cordiner, T. J. Millar, A. J. Markwick-Kemper and P. R. Jewell, *Astrophys. J.*, 2007, **664**, L47–L50.
11 N. Sakai, T. Sakai, Y. Osamura and S. Yamamoto, *Astrophys. J.*, 2007, **667**, L65–L68.
12 E. Herbst and Y. Osamura, *Astrophys. J.*, 2008, **679**, 1670–1679.
13 T. R. Taylor, C. S. Xu and D. M. Neumark, *J. Chem. Phys.*, 1998, **108**, 10018–10026.

14 J. Zhou, E. Garand and D. M. Neumark, *J. Chem. Phys.*, 2007, **127**, 114313.
15 J. Zhou, E. Garand and D. M. Neumark, *J. Chem. Phys.*, 2007, **127**, 154320.
16 S. M. Sheehan, B. F. Parsons, T. A. Yen, M. R. Furlanetto and D. M. Neumark, *J. Chem. Phys.*, 2008, **128**, 174301.
17 S. M. Sheehan, B. F. Parsons, J. Zhou, E. Garand, T. A. Yen, D. T. Moore and D. M. Neumark, *J. Chem. Phys.*, 2008, **128**, 034301.
18 P. Freivogel, J. Fulara, M. Jakobi, D. Forney and J. P. Maier, *J. Chem. Phys.*, 1995, **103**, 54–59.
19 M. Kotterer and J. P. Maier, *Chem. Phys. Lett.*, 1997, **266**, 342–346.
20 H. Linnartz, T. Motylewski and J. P. Maier, *J. Chem. Phys.*, 1998, **109**, 3819–3823.
21 H. Linnartz, T. Motylewski, O. Vaizert, J. P. Maier, A. J. Apponi, M. C. McCarthy, C. A. Gottlieb and P. Thaddeus, *J. Mol. Spectrosc.*, 1999, **197**, 1–11.
22 H. Ding, T. Pino, F. Guthe and J. P. Maier, *J. Chem. Phys.*, 2001, **115**, 6913–6919.
23 H. Ding, T. Pino, F. Guthe and J. P. Maier, *J. Chem. Phys.*, 2002, **117**, 8362–8367.
24 J. Fulara, D. Lessen, P. Freivogel and J. P. Maier, *Nature*, 1993, **366**, 439–441.
25 M. Grutter, M. Wyss and J. P. Maier, *J. Chem. Phys.*, 1999, **110**, 1492–1496.
26 M. Tulej, F. Guthe, M. Schnaiter, M. V. Pachkov, D. A. Kirkwood, J. P. Maier and G. Fischer, *J. Phys. Chem. A*, 1999, **103**, 9712–9716.
27 T. Pino, M. Tulej, F. Guthe, M. Pachkov and J. P. Maier, *J. Chem. Phys.*, 2002, **116**, 6126–6131.
28 C. A. Gottlieb, E. W. Gottlieb and P. Thaddeus, *Astron. Astrophys.*, 1986, **164**, L5–L6.
29 J. C. Pearson, C. A. Gottlieb, D. R. Woodward and P. Thaddeus, *Astron. Astrophys.*, 1988, **189**, L13–L15.
30 M. C. McCarthy, M. J. Travers, P. Kalmus, C. A. Gottlieb and P. Thaddeus, *Astrophys. J.*, 1996, **467**, L125–L127.
31 M. C. McCarthy, M. J. Travers, A. Kovacs, C. A. Gottlieb and P. Thaddeus, *Astron. Astrophys.*, 1996, **309**, L31–L33.
32 M. J. Travers, M. C. McCarthy, C. A. Gottlieb and P. Thaddeus, *Astrophys. J.*, 1996, **465**, L77–L80.
33 M. C. McCarthy, M. J. Travers, A. Kovacs, C. A. Gottlieb and P. Thaddeus, *Astrophys. J. Suppl.*, 1997, **113**, 105–120.
34 M. C. McCarthy, W. Chen, A. J. Apponi, C. A. Gottlieb and P. Thaddeus, *Astrophys. J.*, 1999, **520**, 158–161.
35 A. J. Apponi, M. E. Sanz, C. A. Gottlieb, M. C. McCarthy and P. Thaddeus, *Astrophys. J.*, 2001, **547**, L65–L68.
36 M. C. McCarthy and P. Thaddeus, *J. Chem. Phys.*, 2005, **122**, 174308.
37 H. Gupta, S. Brunken, F. Tamassia, C. A. Gottlieb, M. C. McCarthy and P. Thaddeus, *Astrophys. J.*, 2007, **655**, L57–L60.
38 C. Barckholtz, T. P. Snow and V. M. Bierbaum, *Astrophys. J.*, 2001, **547**, L171–L174.
39 Y. Shi and K. M. Ervin, *J. Phys. Chem. A*, 2008, **112**, 1261–1267.
40 D. E. Woon, *Chem. Phys. Lett.*, 1995, **244**, 45–52.
41 A. L. Sobolewski and L. Adamowicz, *J. Chem. Phys.*, 1995, **102**, 394–399.
42 S. Dua, J. C. Sheldon and J. H. Bowie, *J. Chem. Soc., Chem. Commun.*, 1995, 1067–1068.
43 T. D. Crawford, J. F. Stanton, J. C. Saeh and H. F. Schaefer, *J. Am. Chem. Soc.*, 1999, **121**, 1902–1911.
44 J. Haubrich, M. Muhlhauser and S. D. Peyerimhoff, *J. Phys. Chem. A*, 2002, **106**, 8201–8206.
45 L. Pan, B. K. Rao, A. K. Gupta, G. P. Das and P. Ayyub, *J. Chem. Phys.*, 2003, **119**, 7705–7713.
46 S. J. Blanksby, S. Dua and J. H. Bowie, *J. Phys. Chem. A*, 1999, **103**, 5161–5170.
47 Z. X. Cao and S. D. Peyerimhoff, *Phys. Chem. Chem. Phys.*, 2001, **3**, 1403–1406.
48 P. Botschwina and R. Oswald, *Int. J. Mass Spectrom.*, 2008, **277**, 180–188.
49 P. Botschwina, R. Oswald, G. Knizia and H. J. Werner, *Z. Phys. Chem.*, 2009, **223**, 447–460.
50 F. Pichierri, *J. Phys. Chem. A*, 2008, **112**, 7717–7722.
51 M. L. Senent and M. Hochlaf, *Astrophys. J.*, 2010, **708**, 1452–1458.
52 C. Ochsenfeld, R. I. Kaiser, Y. T. Lee, A. G. Suits and M. HeadGordon, *J. Chem. Phys.*, 1997, **106**, 4141–4151.
53 S. Dua, J. H. Bowie and S. J. Blanksby, *Eur. J. Mass Spectrom.*, 1999, **5**, 309–317.
54 R. F. Curl, P. G. Carrick and A. J. Merer, *J. Chem. Phys.*, 1985, **82**, 3479–3486.
55 K. M. Ervin and W. C. Lineberger, *J. Phys. Chem.*, 1991, **95**, 1167–1177.
56 D. M. Neumark, *J. Phys. Chem. A*, 2008, **112**, 13287.
57 A. Osterwalder, M. J. Nee, J. Zhou and D. M. Neumark, *J. Chem. Phys.*, 2004, **121**, 6317–6322.
58 M. J. Nee, A. Osterwalder, J. Zhou and D. M. Neumark, *J. Chem. Phys.*, 2006, **125**, 014306.
59 D. W. Chandler and P. L. Houston, *J. Chem. Phys.*, 1987, **87**, 1445–1447.
60 A. Eppink and D. H. Parker, *Rev. Sci. Instrum.*, 1997, **68**, 3477–3484.
61 U. Even, J. Jortner, D. Noy, N. Lavie and C. Cossart-Magos, *J. Chem. Phys.*, 2000, **112**, 8068–8071.
62 E. Garand, T. I. Yacovitch and D. M. Neumark, *J. Chem. Phys.*, 2009, **130**, 064304.
63 E. W. Hansen and P. L. Law, *J. Opt. Soc. Am. A*, 1985, **2**, 510–520.
64 J. C. Rienstra-Kiracofe, G. S. Tschumper, H. F. Schaefer, S. Nandi and G. B. Ellison, *Chem. Rev.*, 2002, **102**, 231–282.
65 J. Cooper and R. N. Zare, *J. Chem. Phys.*, 1968, **48**, 942–943.
66 K. L. Reid, *Annu. Rev. Phys. Chem.*, 2003, **54**, 397–424.
67 E. P. Wigner, *Phys. Rev.*, 1948, **73**, 1002–1009.
68 C. T. Lee, W. T. Yang and R. G. Parr, *Phys. Rev. B*, 1988, **37**, 785–789.
69 A. D. Becke, *J. Chem. Phys.*, 1993, **98**, 1372–1377.
70 T. H. Dunning, *J. Chem. Phys.*, 1989, **90**, 1007–1023.
71 M. J. Frisch, G. W. Trucks, H. B. Schlegel, G. E. Scuseria, M. A. Robb, J. R. Cheeseman, J. A. Montgomery, Jr., T. Vreven, K. N. Kudin, J. C. Burant, J. M. Millam, S. S. Iyengar, J. Tomasi, V. Barone, B. Mennucci, M. Cossi, G. Scalmani, N. Rega, G. A. Petersson, H. Nakatsuji, M. Hada, M. Ehara, K. Toyota, R. Fukuda, J. Hasegawa, M. Ishida, T. Nakajima, Y. Honda, O. Kitao, H. Nakai, M. Klene, X. Li, J. E. Knox, H. P. Hratchian, J. B. Cross, V. Bakken, C. Adamo, J. Jaramillo, R. Gomperts, R. E. Stratmann, O. Yazyev, A. J. Austin, R. Cammi, C. Pomelli, J. Ochterski, P. Y. Ayala, K. Morokuma, G. A. Voth, P. Salvador, J. J. Dannenberg, V. G. Zakrzewski, S. Dapprich, A. D. Daniels, M. C. Strain, O. Farkas, D. K. Malick, A. D. Rabuck, K. Raghavachari, J. B. Foresman, J. V. Ortiz, Q. Cui, A. G. Baboul, S. Clifford, J. Cioslowski, B. B. Stefanov, G. Liu, A. Liashenko, P. Piskorz, I. Komaromi, R. L. Martin, D. J. Fox, T. Keith, M. A. Al-Laham, C. Y. Peng, A. Nanayakkara, M. Challacombe, P. M. W. Gill, B. G. Johnson, W. Chen, M. W. Wong, C. Gonzalez and J. A. Pople, *GAUSSIAN 03 (Revision C.02)*, Gaussian, Inc., Wallingford, CT, 2004.
72 K. M. Erwin, FCFgauss03: Gaussian 03 output conversion program, 2004.
73 K. M. Erwin, PESCAL, Fortran program, 2008.
74 P. Chen, in *Unimolecular and Bimolecular Reaction Dynamics*, ed. T. Baer, C.-Y. Ng and I. Powis, John Wiley & Sons, Chichester, 1994, pp. 371–425.
75 F. Duschinsky, *Acta Physicochim. URSS*, 1937, **7**, 551–566.
76 S. J. Blanksby, A. M. McAnoy, S. Dua and J. H. Bowie, *Mon. Not. R. Astron. Soc.*, 2001, **328**, 89–100.
77 E. Garand, T. I. Yacovitch and D. M. Neumark, *J. Chem. Phys.*, 2008, **129**, 074312.
78 E. Garand, T. I. Yacovitch and D. M. Neumark, *J. Chem. Phys.*, 2009, **131**, 054312.